


RESEARCH ARTICLE

Open Access



Metallurgical and corrosion characterization of warring states period bronzes excavated from Pujiang, Chengdu, China

Liu Liu^{1†}, Qing Zhong^{2†}, Luman Jiang³, Pei Li³, Lin Xiao³, Yangmin Gong³, Zhanyun Zhu^{4,5*}  and Junchang Yang^{2,4,6*}

Abstract

Located in Pujiang, Chengdu, China, more than four hundred artifacts were unearthed during the excavation of the Warring States (the Warring States period lasts from 475 to 221 BC) ship-shaped graves in 2016. The compositional and metallurgical feature of the unearthed vessels are still unclear. Archaeologists and conservators are puzzled by such problems that need to be answered by systematic scientific studies. Fifty one samples, either from the matrix (26 samples), or from the corrosion part (25 samples) of 25 unearthed bronze vessels, were carefully collected from the fallen part of the bronze vessels for analysis. Technical methods, such as OM, SEM-EDS, XRD and Raman Spectroscopy were adopted for compositional and metallurgical characterization of the bronzes, as well as identification of the corrosion products. The bronzes are Cu–Sn–Pb ternary alloys with typical casting microstructure. The proportion of Sn are in accordance with excavated bronze vessels in surrounding areas. Recycling isn't involved with the production of such vessels. Layered structure of the corrosion products was observed. Different corrosion products were identified as $\text{Cu}_2\text{CO}_3(\text{OH})_2$, Cu_2O , $\text{CuSO}_4 \cdot 5\text{H}_2\text{O}$, SnO_2 , PbSO_4 and PbCO_3 . The findings help us gain insights into the bronze manufacturing in Bashu district, as well as the corrosion behavior in certain condition.

Keywords: The Warring States Period, Bronze vessel, Metallurgical characterization, Compositional analysis

Introduction

As a significant center of ancient civilization of China, plenty of the Warring States period bronzes were unearthed in Chengdu Plains. The bronzes play an important role of “Bashu Culture”. More than half of the unearthed bronzes are weapons [1, 2].

Apart from the weapons, bronze vessel, served as an important part of burial objects in Bashu district,

contributing significantly to the study of funeral regulation, as well as the organization of ancient social order. Bronze vessels were excavated from 134 tombs out of 559 in Bashu district, up to 252 pieces. Different type of vessels were unearthed, bronze vessel “Mou” (鬲) was found in 122 tombs, mainly distributed among Chengdu Plains and Eastern Sichuan ridge-valley area [3]. Bronze vessel “Mou” was excavated in central China, originated from Chengdu Plains and spread over surrounding areas. Sichuan Province owns the largest number and clearest series of such archaeological findings. Bronze “Mou” was placed together with other cooking vessels in the tombs. Traces of burning were found in the bottom of the vessel, residues of animal bones were found inside the vessel, indicating the vessel was used for cooking. Bronze vessel “Mou” was buried with regular number in the tombs of certain level, proving it was also treated as ritual vessel [4,

[†]Liu Liu and Qing Zhong contributed equally to this work

*Correspondence: zhanyun.zhu@xmu.edu.cn; yangjunchang@nwpu.edu.cn

² State Key Laboratory of Solidification Processing, Center for Nano Energy Materials, School of Materials Science and Engineering, Northwestern Polytechnical University, Xi'an 710072, China

⁴ Research and Practice Base of Conservation Science and Engineering, Department of History, College of Humanities, Xiamen University, Xiamen 361005, China

Full list of author information is available at the end of the article

5]. Typological study of Mou indicates its type varies in time and region from Qin Dynasty to the Warring States.

During the excavation of Pujiang ship-shaped graves in 2016, several bronze “Mou” with severe corrosion were unearthed together with other bronzes. It would be of interest to study the compositional and metallurgical feature of the unearthed vessels, as well as the characterization of corrosion products. Archaeologists and conservators are puzzled by such problems that need to be answered by systematic scientific studies. Different scientific methods have been applied to the research of bronzes, for a better understanding of their alloy ratio, metallurgical characterization and corrosive behavior [6–8]. Studies on the development of society, technology and military have been conducted by archaeologist according to the period and category of the unearthed bronzeware [9]. Technical analysis of the bronzes in Bashu district has been concentrating on unearthed weapons, revealed bronze production in the ancient Chengdu Plains [10–12], as well as special craft adopted during manufacturing [13]. Few study of bronze vessel “Mou” has been reported.

The unearthed bronze vessels in Pujiang County are served as a precious material for a better understanding of the bronze manufacturing technology of Chengdu Plains in the Warring States period. Technical methods, such as OM, SEM-EDS, XRD and Raman Spectroscopy were adopted for the research, for a better understanding of compositional and metallurgical characterization of the bronze vessel, as well as the identification of the corrosion products.

Archaeological context

Located in the southwest of Sichuan Basin in China, Pujiang County (80 km to Chengdu City) experienced the excavation of 60 tombs from the late Warring States period in 2016 (Fig. 1). The tombs are divided into three different types according to their sizes with the length up to 9-m, 6-m and 3-m, respectively. Several ship-shaped coffins were found with the length from 4 to 7 m and the width from 0.9 to 2 m. The coffin was made by curving the wood into the shape of the ship. More than four hundred ancient artifacts were unearthed, including 12 seals with the interpretation of “Bashu”, 2 eyebeads, lacquerwares, potteries and bronzes. The number of bronzes exceeds 45% of the artifacts. The bronzes consist of different categories, including vessel, weapon, tool, coin and ornament. Bronze vessel Fu (釜) and bronze vessel Mou (盩) were identified. Unfortunately, most of the bronzewares are broken and are suffering from severe corrosion. For the first time, the character “Cheng Du”, carved on a bronze spear in tomb M32, was identified in Chengdu

area. This is potentially indicative of a recognition by local citizens in the late Warring States period [14].

The ancient citizens lived along river, therefore buried in a ship-shaped coffin with bronzes, lacquerware and pottery was usual through the Warring States period [15]. Another ship-shaped coffin was excavated in Pujiang in 1998 with 51 pottery, bronzeware and woodware [16]. There are different opinions about the origin of “Ba” and “Shu”, the culture varies a little bit though they are adjacent, which also reflects by the unearthed bronzes in ship coffins [17].

Material and methods

Material

Twenty five unearthed bronze vessels (bronze “Mou”) dated to the late Warring States period were adopted for the research. 51 samples, both from the matrix (26 samples) and the corrosion part (25 samples) of each bronze vessel, were carefully collected under microscope to ensure its full structure, and therefore are considered to be representative of the vessel. The size of the collected samples was strictly controlled to minimize the adverse impact for restoration (less than 0.5×0.5 cm). Basic information is shown as Table 1. PJ 19 and PJ 21 comes from the top and bottom of the matrix of M11:1. The size and the weight of each vessel were measured accordingly. The bronzes are in poor condition, most of which are suffering from corrosion and incompleteness.

Methods

Microscopic analysis

Observation of the samples was conducted by two microscopes (Axio Scope A1 equipped with ICCS optical system, Zeiss Ltd., Germany and a three-dimensional digital microscope VK-X250, Keyence Corporation, Japan) with the magnification from 50 to 200 \times and 20 to 200 \times .

Metallographic analysis

The metallographic observation was conducted on 26 samples collected from the matrix of the vessels. Samples were embedded by a metallographic inlaying machine (CitoVac, Struers Ltd., Denmark), ground and polished by a Tegramin-20 automatic grinding and polishing equipment (Struers Ltd., Denmark) according to the standard metallographic procedures to achieve the cross-section of the samples. A polarizing microscope (Axio Scope A1, Zeiss Ltd., Germany) was used to observe the cross-section before and after etching with aqueous ferric chloride alcohol solution with the magnification from 50 to 200 \times . All the solvents were purchased from Sinapharm Chemical Reagent CO., analytical grade. The collected samples were observed directly under microscope to record its corrosion product. SEM-EDS analysis



Fig. 1 Map of the excavated site

was conducted with a FEI Verios 4G SEM coupled with an Oxford X-max 20 EDS analyzer to obtain secondary electron (SEM) images and backscattered electron (BSE) images for phase studies. The embed samples with cross-section were analyzed before etching. Samples were analyzed with 10–20 kV acceleration voltage and 8–9 mm working distance.

Compositional analysis

SEM–EDS analysis was conducted with a FEI Verios 4G SEM coupled with an Oxford X-max 20 EDS analyzer was also hired for the characterization of chemical composition. Matrix (cross-section) and corrosion samples were analyzed with 10–20 kV acceleration voltage and 8–9 mm working distance. Industrial copper reference sample was used for calibration and optimization before

Table 1 Basic information of collected samples











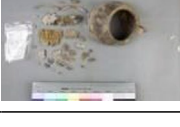
Sample no.	Vessel no.	Size (cm)	Weight (g)	Status	Bronze vessel (Mou)
PJ 13 (matrix) PJ 14 (corrosion)	M1:1	Diameter: 10.3–14.2; height: 12.2; thickness: 0.35	645.6	Nearly complete	
PJ 15 (matrix) PJ 16 (corrosion)	M8: 8	Diameter: 11.9–17.2; height: 15.2; thickness: 0.25	525.2	Incomplete	
PJ 17 (matrix) PJ 18 (corrosion)	M49:16	Diameter: 12.4–17.8; height:16.6; thickness: 0.3	540.7	Nearly complete	
PJ 19 (matrix-top) PJ 21 (matrix-bottom) PJ 20 (corrosion)	M11:1	Diameter: 9.6–13.1; height:12.1; thickness: 0.2	297.1	Nearly complete	
PJ 23(matrix) PJ 24 (corrosion)	M6:12	Diameter: 8.2–12.1; height:11.5; thickness: 0.3	204.4	Nearly complete	
PJ 25 (matrix) PJ 26 (corrosion)	M20:2	Major axis: 13.7; minor axis: 12.3; height: 8.9	153.4	Incomplete	
PJ 27 (matrix) PJ 28 (corrosion)	M47:1	Diameter: 12.0–17.5; height: 15.8; thickness: 0.35	876.0	Nearly complete	
PJ 29 (matrix) PJ 30 (corrosion)	M46:1	Diameter: 12.1–17.7; height: 16.1; thickness: 0.35	613.2	Nearly complete	
PJ 31 (matrix) PJ 32 (corrosion)	M38:5	–	189.7	Fragments	
PJ 33 (matrix) PJ 34 (corrosion)	M41:4	–	–	Fragments	
PJ 35 (matrix) PJ 36 (corrosion)	M13:18	Major axis: 17.0; minor axis: 14.0; height: 14.0	376.6	Incomplete	

Table 1 (continued)












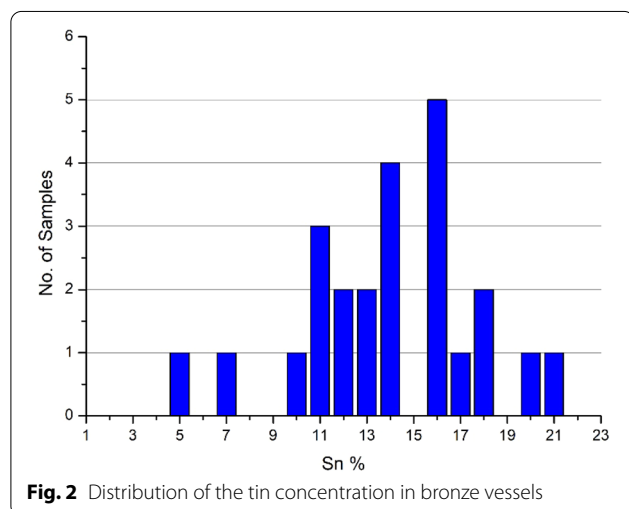
Sample no.	Vessel no.	Size (cm)	Weight (g)	Status	Bronze vessel (Mou)
PJ 37 (matrix) PJ 38 (corrosion)	M44:1	Major axis:12.3; minor axis:11.9; height: 9.6	191.1	Incomplete	
PJ 39 (matrix) PJ 40 (corrosion)	M5:4	Major axis:13.5; minor axis:13.4; thickness: 0.2	93.4	Fragments	
PJ 41 (matrix) PJ 42 (corrosion)	M17:2	Major axis:15.5; minor axis:14.3; thickness: 0.1	120.8	Incomplete	
PJ 43 (matrix) PJ 44 (corrosion)	M39:3	–	627.8	Fragments	
PJ 45 (matrix) PJ 46 (corrosion)	M53:5	Major axis:16.6; minor axis:16.1; height: 14.6	581.0	Incomplete	
PJ 47 (matrix) PJ 48 (corrosion)	M16:6	Thickness:0.15–0.2	162.5	Fragments	
PJ 49 (matrix) PJ 50 (corrosion)	M60:1	Major axis:13.6; minor axis:13.4; height: 11.6	492.6	Incomplete	
PJ 51 (matrix) PJ 52 (corrosion)	M30:6	Major axis:15.3; minor axis:15.1; height: 14.7	667.5	Nearly complete	
PJ 53 (matrix) PJ 54 (corrosion)	M19:1	–	309.3	Fragments	
PJ 55 (matrix) PJ 56 (corrosion)	M56:5	–	228.2	Fragments	
PJ 57 (matrix) PJ 58 (corrosion)	M27:4	Length: 11.3; width: 4.9; height: 0.2	26.1	Fragment	

Table 1 (continued)

Sample no.	Vessel no.	Size (cm)	Weight (g)	Status	Bronze vessel (Mou)
PJ 59 (matrix) PJ 60 (corrosion)	M33:9	–	189.8	Fragments	
PJ 61 (matrix) PJ 62 (corrosion)	M32:5	Major axis: 20.2; minor axis:18.5; height: 15.3	–	Incomplete	
PJ 63 (matrix) PJ 64 (corrosion)	M23	Length:4.2; width:1.7; thickness: 0.1	3.1	Fragment	



analysis. Mapping scanning was adopted during element analysis by EDS in order to minimize the detection error. The area with Pb particle and corrosion were avoided while selecting the detection zone. For the EDS analysis of inclusions and special phase, dot scanning was preferred for accurate results. Each sample was analyzed for three times, the elemental results detected were averaged and normalized.

XRD was performed by a X'Pert Pro MPD diffractometer (Philips, Netherlands) equipped with a Cu-K α radiation source ($\lambda = 0.15418$ nm) in the range of 5° – 95° , with a tube voltage of 40 kV and a current of 200 mA at a scan rate of 10°min^{-1} . Corrosion samples were ground into powder for analysis. XRD spectra was analyzed and matched by JADE.

A Renishaw inVia RM200 Raman spectrometer coupled with microscope was used for analysis. Measurements

Table 2 Chemical composition of the bronzes

Sample no.	Chemical composition (wt%)			Sample no.	Chemical composition (wt%)		
	Cu	Sn	Pb		Cu	Sn	Pb
PJ13	75.42	17.22	7.36	PJ41	83.77	7.49	8.74
PJ15	81.06	13.17	5.77	PJ43	73.53	18.42	8.05
PJ17	75.88	14.43	9.69	PJ45	74.81	16.85	8.34
PJ19	70.88	12.80	16.32	PJ47	71.51	16.12	12.37
PJ23	82.21	11.36	6.43	PJ49	80.27	14.65	5.08
PJ25	72.84	18.23	8.93	PJ51	78.53	16.78	4.69
PJ27	74.80	14.33	10.87	PJ53	65.50	21.35	13.15
PJ29	71.45	16.40	12.15	PJ55	84.27	11.63	4.10
PJ31	75.05	20.52	4.43	PJ57	77.80	11.53	10.67
PJ35	78.05	10.81	11.14	PJ59	84.98	12.99	2.03
PJ37	71.65	14.84	13.51	PJ61	74.15	13.64	12.21
PJ39	83.81	5.11	11.08	PJ63	77.05	16.55	6.40

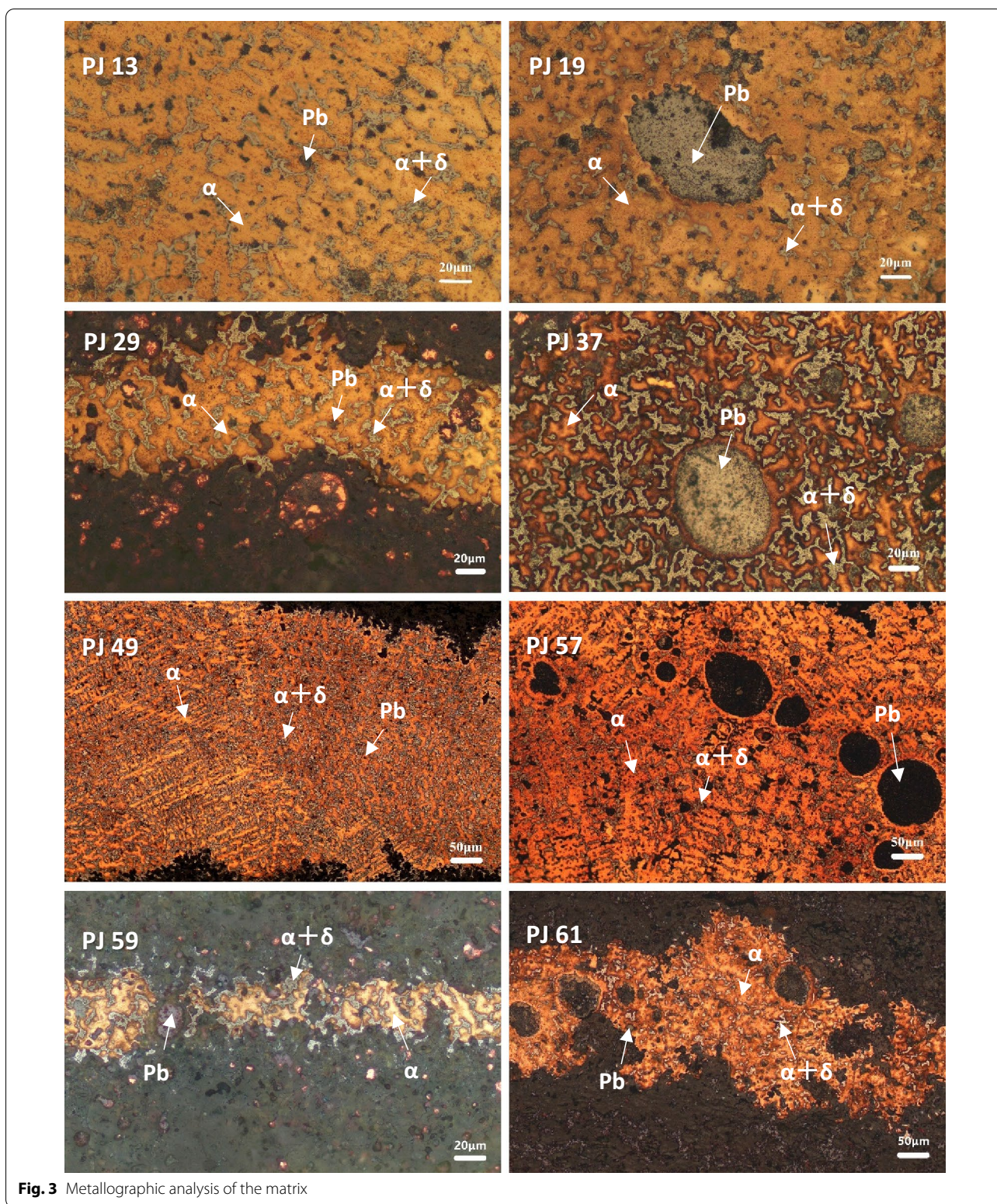


Fig. 3 Metallographic analysis of the matrix

were performed using an argon gas laser at 532 nm with the range 100–3000 cm^{-1} . The detection temperature is 25 °C with the humidity lower than 50%. The spectral resolution was 0.6 cm^{-1} . The laser power was approximately

0.5 mW, which ensured that good quality spectra was recorded. Corrosion samples were placed directly under microscope for the selection of certain corrosion product before detection (Fig. 2).

Results and discussion

Analysis of the matrix

The SEM-EDS analysis of the matrix indicates the bronzes are Cu–Sn–Pb ternary alloys, the proportion of Cu, Sn and Pb differs from 65–85%, 5–22% to 2–17%, respectively (Table 2). The data has been treated with main elements for comparison. It has been generally recognized tin bronze refers to a copper-based alloy containing 2% tin or over, a Cu–Sn–Pb ternary alloy contains both tin and lead at the level of 2% or more [18, 19]. Therefore, the bronzes excavated from Pujiang are tin–lead bronze. Compared with the published data of the Warring States, the composition of the bronze vessels is basically Cu–Sn–Pb, different from the Cu–Pb or Cu–Sn binary alloys found in bronze weapon and ornament. The proportion of Sn concentrates between 10 and 18%, which is in accordance with the bronze vessels in Baishoulu, Shu State [11]. The cemetery of Xindu, Majia, 100 km northeastern to Pujiang, is a late Warring States-period tomb in Bashu district. The ratio of Sn of Majia bronze vessels varies from 6 to 20%, with an 8.7% found in bronze Mou [20]. Therefore, the Warring States bronze vessel in Chengdu Plains and surrounding areas are made to a specific designed composition. The variation of the Sn concentration might have a relation with the tomb owner’s social status [21]. The lead sources of the vessels are still unclear, which could be reported by further studies to explain the bronze flow in ancient time.

A method has been established to infer whether the bronzes in a certain region are primary alloys or contain recycled metal by considering the shape of the

distribution of the tin concentrations within the assemblage. Thus a unimodal approximately normal distribution of tin centered around 10–20% indicates the assemblage is likely to be made of a primary alloy [22]. The distribution of tin concentration of bronze Mou peaks at 16, indicating recycled alloy was not adopted in this case.

Metallurgical observation of the cross-section presents typical casting microstructure, further processing during manufacturing didn’t appear according to the metallographic analysis. Different from the weapons in ancient Chengdu Plains, the vessels were cast without secondary processing [12]. Part of the metallographic observation was shown in Fig. 3, presenting a dendritic microstructure. The ($\alpha + \delta$) eutectoid was uniformly distributed among the dendritic microstructure. Lead inclusions shows random distribution [12, 19]. The bronze samples are suffering from heavily mineralization, PJ59 presents layered structure with little bronze matrix remains. Samples of PJ17/PJ23/PJ29 and PJ41 are nearly in the same condition. Small holes and cracks, as well as dendritic segregation, appear in both matrix and corrosion product. A few blue-grey inclusions are visible, shaped as small and big particles, diffusely distributed among δ solid solution and outside($\alpha + \delta$)eutectoid. For other samples with less mineralization, small holes and cracks are concentrating among the corrosion layer.

BSE images of the samples are attached as Additional file 1: Fig. S1. Element distribution of each microstructure was detected, taking PJ59 as an example (Fig. 4 and Table 3): Two different metallographic phases, α phase

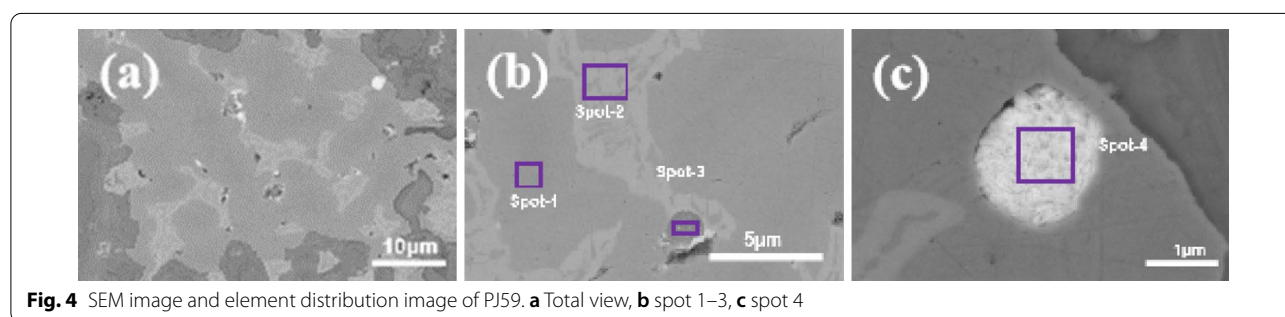


Fig. 4 SEM image and element distribution image of PJ59. **a** Total view, **b** spot 1–3, **c** spot 4

Table 3 The chemical composition of PJ59

No.	Chemical composition (SEM-EDS, wt%)						
	C	O	S	Cu	Sn	Pb	
Spot-1	1.40	0.52	–	89.54	8.53	–	
Spot-2	1.05	–	–	74.39	24.56	–	
Spot-3	2.62	–	19.08	78.30	–	–	
Spot-4	3.03	8.00	–	–	–	88.96	

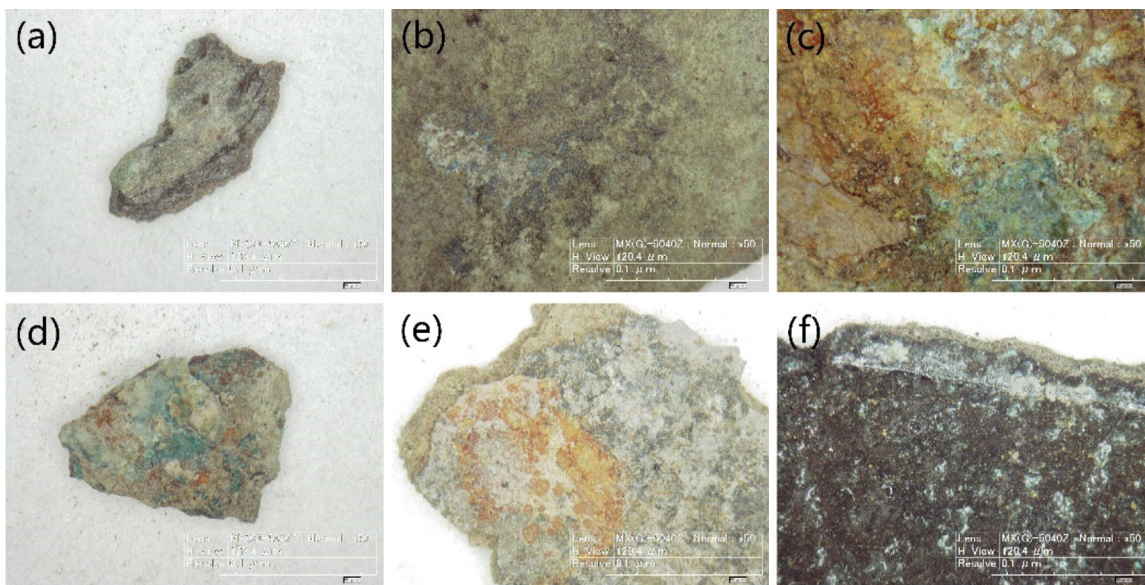


Fig. 5 Photo of corrosion samples. **a** M1:1, **b** M8:8, **c** M49:16, **d** M11:1, **e** M41:4, **f** M16:6

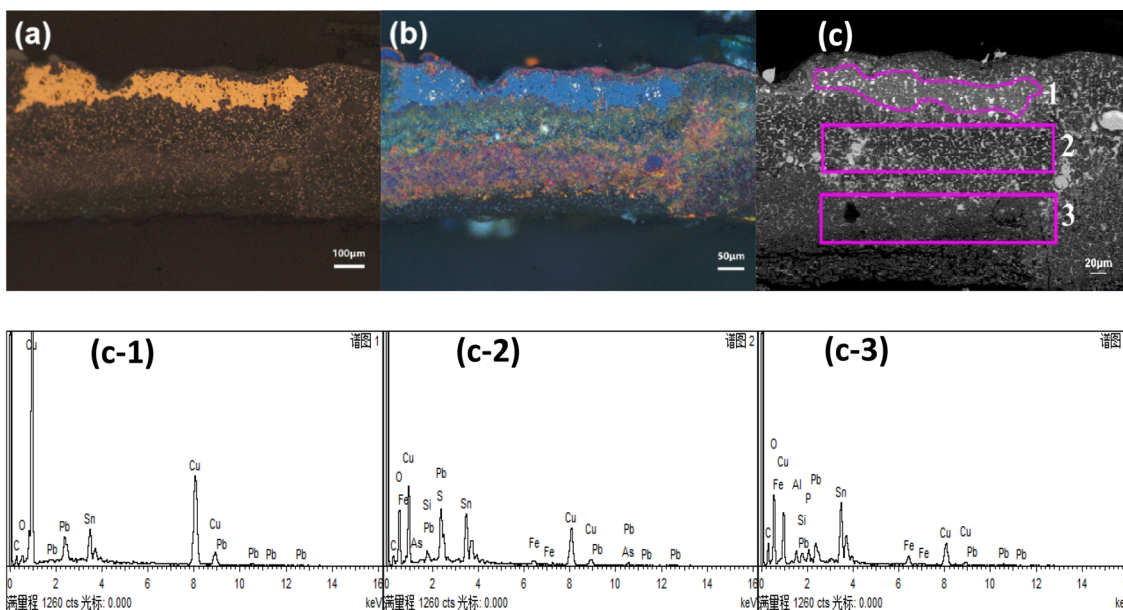


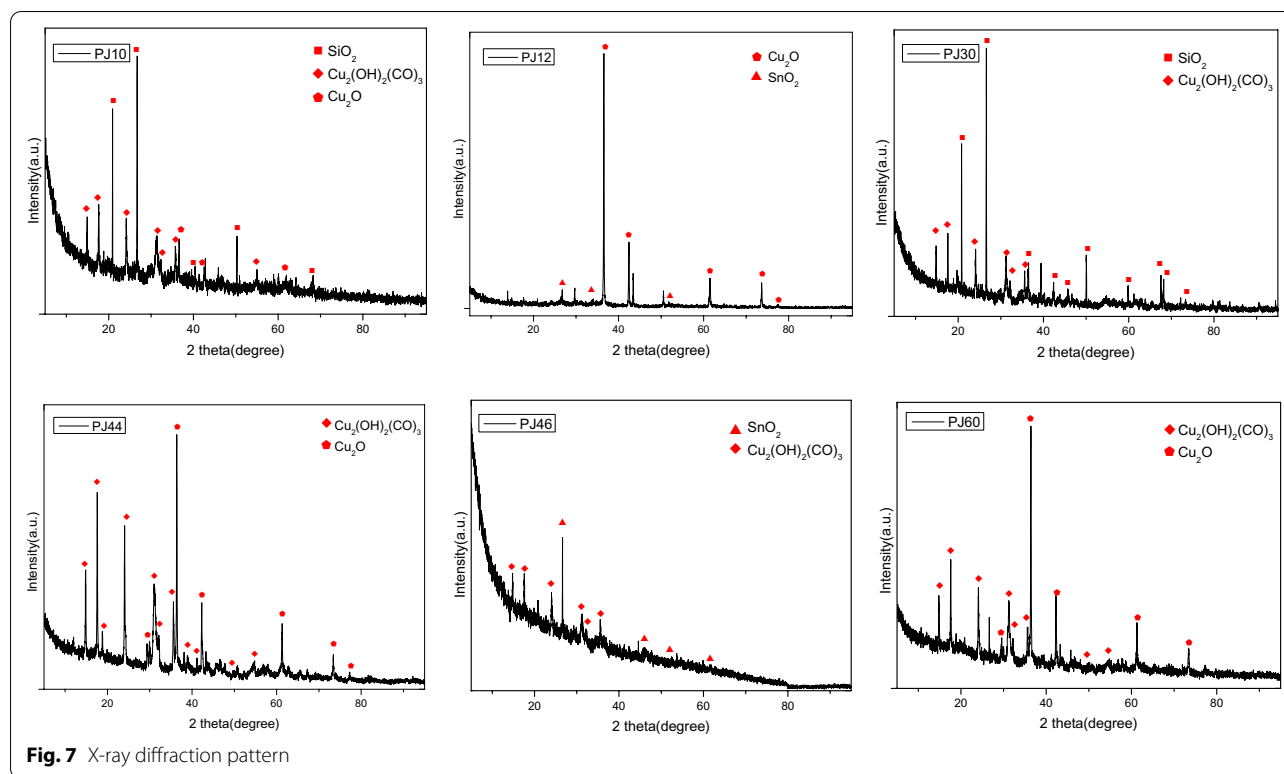
Fig. 6 **a** Sample of PJ17, **b** OM images, **c** SEM-BSE image. **c-1–c-3** EDS analysis of zone 1–3

(Spot-1) and $(\alpha + \delta)$ phase (Spot-2) were observed based on the BSE mode of SEM, while white lead particle was visible (Spot-4). The proportion of Cu and Sn differs in different phases. The dark particle in Spot-3, observed as blue-grey inclusions in metallographic analysis, contains Cu and S. Apart from fully mineralization samples, sulphide was frequently identified.

Analysis of the corrosion products

Different corrosion products are shown in Fig. 5, appear as yellow, black, orange, green, grey and red mineral. The microscopic observation indicates the corrosion products exist in the form of smooth and dense layer with cracks.

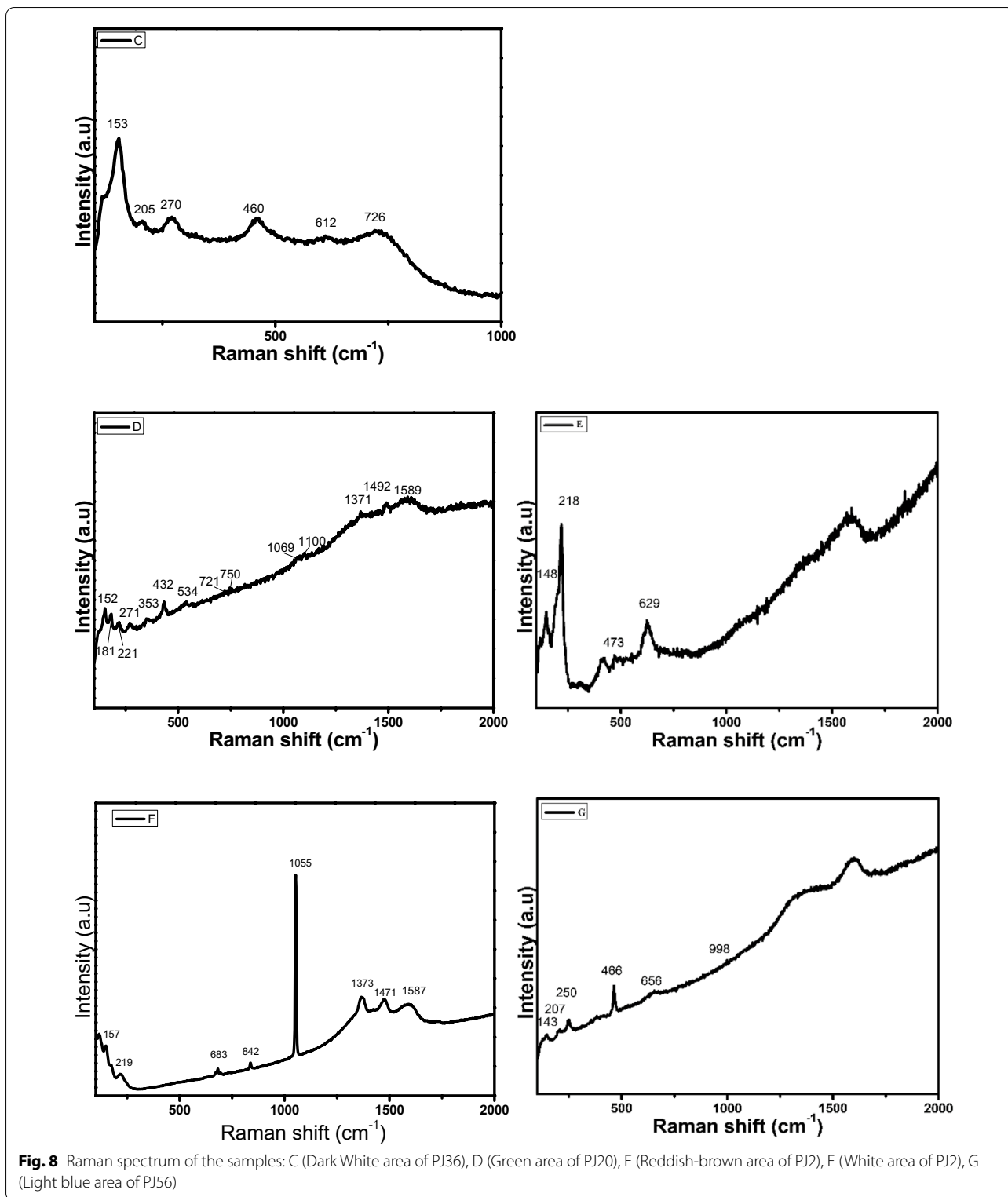
Seven embedded matrix samples with full structure were analyzed by SEM-EDS for a better understanding



of corrosion status. Layered structure of the corrosion products was obviously noticed under microscope, presented as matrix layer and corrosion layer with unclear boundary. Corrosion appears in the matrix layer as well. Apart from Cu, Sn and Pb, elements such as Si, P, Fe and As were identified in the corrosion layer, indicates mineralization starts during corrosion. The content of Cu decreases from inner layer to the surface layer, demonstrating corrosion starts from the surface. The main element in the corrosion layer is Sn, followed by Cu, which is the characteristic of “tin-rich” corrosion layer [23]. “Tin-rich” corrosion layer, often considered appears in the bronze mirror or weapons with a Sn concentration exceeds 17%, was found in the bronze vessels with the Sn concentration varies from 12 to 17% in this case. Two different corrosion layers were observed in PJ17, shown as red corrosion layer and green corrosion layer from inside to the outside (Fig. 6). The composition differs in each layer according to the elements detected by EDS. Cu, Sn and Pb were detected in zone 1. Elements such as Cu, Sn, Pb, S, Fe, Si and As were found in zone 2. Cu, Sn, Pb, Si, Fe and Al were identified in zone 3. According to the previous research, the corrosion products consists of outer layer (mineralized layer) and inner layer (altered zone). The outer layer possesses a stable Cu/Sn ratio with element from burial environment. The inner layer has a higher proportion of Cu, and couldn't be observed in

every sample [24–26]. Fortunately, element Cl wasn't detected by EDS, indicates that copper hydroxychlorides, which will cause “bronze diseases”, didn't appear in the corrosion products [27].

The bronzes were buried underground for thousands of years and were subject to corrosion due to the interaction with water, oxygen and carbon dioxide [28–30]. Micro-Raman spectroscopy and XRD were adopted to identify the chemical composition of the corrosion products. $\text{Cu}_2\text{CO}_3(\text{OH})_2$ (PDF#72-0075) and Cu_2O (PDF#78-2076) are the most common minerals among corrosion products. Besides, SnO_2 (PDF#72-1147) and SiO_2 (PDF#87-2096) were identified in some samples by XRD detection (Fig. 7). SnO_2 was frequently identified on the surface of ancient corroded bronzes. Analysis by SEM-EDS shows a significant higher content of Sn and a lower content of Cu in the corrosion layer compared to the matrix layer. Such patina was formed according to the “natural corrosion mechanism” with two key factors played important roles, i.e., high Sn content and the damp, wet and acid burial conditions [31], which is in accordance with previous discussion. The formation of SnO_2 comes from the selective corrosion [32]. Tin oxides are easier formed than cuprous oxides [33]. The loss of Cu results in the enrichment of Sn on the surface [34].



Tested samples by Raman spectrometer shown different minerals (Fig. 8). The presence of cuprite (Cu₂O) can be concluded from spectra of reddish-brown

minerals (Fig. 8-E), reveals well-resolved bands at 148, 218 and 629 cm⁻¹ [35, 36]. The formation of cuprite layer starts from the early process (before burial) of

bronze oxidation/corrosion by exposure to the open air. Such layer benefits the preservation of bronzes due to its dense structure [37, 38]. Green area (Fig. 8-D) with its characteristic absorption in 152, 183, 220, 272, 360, 432, 535, 721, 757, 1065, 1097, 1373, 1498 and 1593 cm^{-1} indicates the existence of malachite [39]. Apart from the cuprite (known as “noble patina”), basic copper carbonates malachite is typically part of the “vile patina”, which usually appears as overlapping secondary corrosion products [27, 40, 41]. The absorption bands of light blue area (Fig. 8-G) in sample PJ56 should be attributed to the vibration of Cu–O and SO_4 in chalcantite ($\text{CuSO}_4 \cdot 5\text{H}_2\text{O}$) [42, 43], with aqueous sulfate tetrahedral oxyanion at 998 cm^{-1} and a complex set of overlapping bands observed at 143, 207 and 250 cm^{-1} . Sulfating corrosion of copper alloys can be observed as pitting corrosion of surfaces exposed to fresh water. For chalcantite to form at any Eh/pH combination, one must have very high concentrations of sulfate and copper [44]. Chalcantite dehydrates over pH 2.5 as well as in atmospheric exposure [45]. The presence of chalcantite indicates the burial environment owns acidity soil with abundant water.

Peaks in 157, 219, 683, 842, 1055, 1373, 1471 and 1587 cm^{-1} (Fig. 8-F) are in accordance with the characterize peaks of PbCO_3 [46]. The characterization peaks (Fig. 8C) also indicates the formation of PbSO_4 [47]. The adding of certain amount of Pb during the bronzes manufacturing is one of the features among the Warring States bronzes. Pb distributes along dendritic crystal as isolated phase, shaped as sphericity and particle in bronzes. Suffering from the CO_2 , O_2 , H_2O and sulphate in the burial environment, the isolated Pb is easily corroded, forming lead corrosion products [48, 49].

Conclusion

The Warring States bronze vessel “Mou” excavated from southwestern China, presents compositional and metallurgical characters which enriches our knowledge of ancient manufacturing. All the collected samples present typical casting microstructure, the ($\alpha + \delta$) eutectoid was uniformly distributed among the dendritic microstructure while lead inclusions shows random distribution. The SEM-EDS analysis indicates the bronzes are Cu–Sn–Pb ternary alloys, the proportion of Cu, Sn and Pb differs from 65–85%, 5–22% to 2–17%, respectively. The Warring States bronze vessel in Chengdu Plains and surrounding areas are made to a specific designed composition, recycling isn’t involved with the production of such vessels. The bronzes are buried in a seasonal environment with acid soil and abundant water. Corrosion happens during the interaction with oxygen, carbon hydrates and water. Layered structure of corrosion products was observed. Different corrosion products were

identified as $\text{Cu}_2\text{CO}_3(\text{OH})_2$, Cu_2O , SnO_2 , PbSO_4 , PbCO_3 and $\text{CuSO}_4 \cdot 5\text{H}_2\text{O}$. The findings help us gain insights into the bronze manufacturing of Bashu district in Warring States period, as well as the corrosion behavior in certain environment. Besides, most of the bronze “Mou” are corroded and broken, the study offers supporting for the conservators during restoration.

Abbreviations

OM: Optical microscope; SEM–EDS: Scanning electron microscopy in combination with energy dispersive X-ray analysis; XRD: X-ray diffraction.

Supplementary Information

The online version contains supplementary material available at <https://doi.org/10.1186/s40494-022-00674-w>.

Additional file 1: Fig. S1. BSE images of the samples.

Acknowledgements

The authors would like to extend their gratitude to Ms. Xiaojuan Dang from Shaanxi Institute for the Preservation of Cultural Heritage, for the technical support during scientific analysis. Useful comments from Dr. Panpan Tan are greatly appreciated. Yangmin Gong is the ex-employee of Chengdu Institute of Cultural Relics and Archaeology.

Authors’ contributions

LL did data analyses and paper writing, ZQ performed the experiments and data analysis. LJ, PL, LX and YG helped with the excavation and sample collection, ZZ and JY reviewed and edited the paper. All authors have read and approved the final manuscript.

Funding

This work was supported by The National Social Science Fund of China (Project No. 19CKG025).

Availability of data and materials

The data and materials used during the study are available from the corresponding author on reasonable requests.

Declarations

Competing interests

The authors declare there is no competing interests.

Author details

¹Xiamen Academy of Arts and Design, Fuzhou University, Xiamen 361000, China. ²State Key Laboratory of Solidification Processing, Center for Nano Energy Materials, School of Materials Science and Engineering, Northwestern Polytechnical University, Xi’an 710072, China. ³Chengdu Institute of Cultural Relics and Archaeology, Chengdu 610042, China. ⁴Research and Practice Base of Conservation Science and Engineering, Department of History, College of Humanities, Xiamen University, Xiamen 361005, China. ⁵Department of Archaeology, Max Planck Institute for the Science of Human History, D-07745 Jena, Germany. ⁶Institute of Culture and Heritage, Northwestern Polytechnical University, Xi’an 710072, China.

Received: 18 November 2021 Accepted: 4 March 2022

Published: 24 March 2022

References

1. Yao Z. Review of bronzes from Bashu area. *Sichuan Cult Relics*. 2004;3:38–45 (In Chinese).

2. Duan Y. Progress of bronze culture in Bashu area. *Cult Relics*. 1996;3:36–47 (In Chinese).
3. Xiang M. Archaeological perspective on Ba's and Shu's ancient histories. Changchun: Jilin University; 2017. (In Chinese).
4. Chen W. Study on bronze Mou. *Archaeol Relics*. 1994;1:66–76 (In Chinese).
5. Men J. Archaeological research on the unearthed cooking boiler of Han tombs in the Xiajiang area. Nanjing: Nanjing University; 2018. (In Chinese).
6. Kareem K, Sultan S, He L. Fabrication, microstructure and corrosive behavior of different metallographic tin-leaded bronze alloys part II: chemical corrosive behavior and patina of tin-leaded bronze alloys. *Mater Chem Phys*. 2016;169:158–72. <https://doi.org/10.1016/j.matchemphys.2015.11.044>.
7. Luo W, Song G, Hu Y, Chen D. Tentative determination of a special bronze material by multiple technological test on a Xuan-Liu dagger-axe from the Xujialing Site, the Eastern Zhou period, Henan Province, China. *J Cult Herit*. 2020;46:304–12. <https://doi.org/10.1016/j.culher.2020.06.016>.
8. Mu D, Luo W, Song G, Qiao B, Wang F. The features as a county of Chu State: chemical and metallurgical characteristics of the bronze artifacts from the Bayilu site. *Archaeol Anthropol Sci*. 2019;11:1123–9. <https://doi.org/10.1007/s12520-018-0596-8>.
9. Sichuan Museum. Bronzes in Bashu area. Chengdu: Chengdu press; 1993. p. 252–4 (In Chinese).
10. Li H, Zuo Z, Cui J, Tian J, Yang Y, Yi L, Zhou Z, Fan J. Bronze production in the Ancient Chengdu Plains: a diachronic metallurgical perspective on a separate cultural region. *J Cult Herit*. 2020;43:26–36. <https://doi.org/10.1016/j.culher.2019.11.005>.
11. Li H, Zuo Z, Cui J, Tian J, Yang Y, Yi L, Zhou Z, Fan J. Copper alloy production in the Warring States period (475–221 BCE) of the Shu state: a metallurgical study on copper alloy objects of the Baishoulu cemetery in Chengdu, China. *Herit Sci*. 2020;8:67. <https://doi.org/10.1186/s40494-020-00412-0>.
12. Li H, Zhou Z, Liu Y, Wang Y, Wang Z, Wang L, Tian J, Cui J. Fighting and burial: the production of bronze weapons in the Shu state based on a case study of Xinghelu cemetery, Chengdu, China. *Herit Sci*. 2020;8:36. <https://doi.org/10.1186/s40494-020-00379-y>.
13. Yao Z, Sun S. Hot tinning of bronze weapons in Bashu area. *J Univ Sci Technol Beijing*. 2007;10:1005–9 (In Chinese).
14. Liu Y, Gong Y. The Warring States ship coffin burials in Pujiang, Chengdu. Year book of archaeology in China. Beijing: China Social Sciences Press; 2017. p. 408 (In Chinese).
15. Tang X. Archaeological research of the Warring States murals in Chengdu Plains. Kunming: Yunnan University; 2016. (In Chinese).
16. Jiang C, Chen Y. Excavation of ship coffin in Pujiang, Chengdu. *Relics*. 2002;4:27–31 (In Chinese).
17. Feng H, Yang Y, Wang J. Ship coffin in ancient Sichuan. *Acta Archaeol Sin*. 1958;2:77–97 (In Chinese).
18. Zhang Z, Ma Q. Compositional and metallurgical characterization of bronzes excavated from Yujawan, Gansu. *Sci Conserv Archaeol*. 2008;1:24–32 (In Chinese).
19. Mei J, Chen K, Cao W. Scientific examination of Shang-dynasty bronzes from Hanzhong, Shaanxi Province, China. *J Archaeol Sci*. 2009;36:1881–91. <https://doi.org/10.1016/j.jas.2009.04.017>.
20. Zeng Z. Analysis of unearthed Bashu bronzes. *Sichuan Relics*. 1992;3:75–7 (In Chinese).
21. Liu R, Pollard AM, Cao Q, Liu C, Sainsbury V, Howarth P, et al. Social hierarchy and the choice of metal recycling at Anyang, the last capital of Bronze Age Shang China. *Sci Rep*. 2020;10:18794. <https://doi.org/10.1038/s41598-020-75920-x>.
22. Pollard AM. Beyond provenance new approaches to interpreting the chemistry of archaeological copper alloys. Leuven: Leuven University Press; 2018.
23. Liu W, Chen J. The advances in the study of tin-rich patina on the surface of ancient bronzes. *J Natl Mus China*. 2019;5:146–60 (In Chinese).
24. Robbiola L, Blengino JM, Fiaud C. Morphology and mechanisms of formation of natural patinas on archaeological Cu & Sn alloys. *Corros Sci*. 1998;12:2083–111. [https://doi.org/10.1016/S0010-938X\(98\)00096-1](https://doi.org/10.1016/S0010-938X(98)00096-1).
25. Meeks N. 6-Patination phenomena on Roman and Chinese high-tin bronze mirrors and other artefacts. *Met Plat Patination*. 1993. <https://doi.org/10.1016/B978-0-7506-1611-9.50010-8>.
26. Wang C, Lu B, Liu X, Xu C, Tan S, Tian L. Research of SnO₂ on ancient black mirror. *Sci China*. 1994;8:840–4 (In Chinese).
27. Scott D. Bronze disease: a review of some chemical problems and the role of relative humidity. *J Am Inst Conserv*. 1990;29:193–206. <https://doi.org/10.1179/019713690806046064>.
28. Albini M, Letardi P, Mathys L, Brambilla L, Schirter J, Junier P, Joseph E. Comparison of a bio-based corrosion inhibitor versus benzotriazole on corroded copper surfaces. *Corros Sci*. 2018;143:84–92. <https://doi.org/10.1016/j.corsci.2018.08.020>.
29. Griesser M, Kockelmann W, Hradil K, Traum R. New insights into the manufacturing technique and corrosion of high leaded antique bronze coins. *Microchem J*. 2016;126:181–93. <https://doi.org/10.1016/j.microc.2015.12.002>.
30. Oudbashi O, Hasanpour A, Davami P. Investigation on corrosion stratigraphy and morphology in some Iron Age bronze alloys vessels by OM, XRD and SEM-EDS methods. *Appl Phys A*. 2016;122:262. <https://doi.org/10.1007/s00339-016-9793-4>.
31. Li B, Jiang X, Wu R, Wei B, Hu T, Pan C. Formation of black patina on an ancient Chinese bronze sword of the Warring States Period. *Appl Surf Sci*. 2018;455:724–8. <https://doi.org/10.1016/j.apsusc.2018.06.024>.
32. Gettens RJ. Tin-oxide patina of ancient high-tin bronze. *Bull Found Art Mus*. 1949;11:16–26.
33. Piccato P, Mille B, Robbiola L. 14-Tin and copper oxides in corroded archaeological bronzes. In: Dillmann P, Beranger G, Piccardo P, Matthiesen H, editors. European Federation of Corrosion (EFC) series, corrosion of metallic heritage artefacts. Sawston: Woodhead Publishing; 2007. p. 239–62. <https://doi.org/10.1533/9781845693015.239>.
34. Sun S, Ma Z, Jin L, Han R, Ke J. The influence of humic acid to the formation of black tin-riched corrosion layer on the surface of bronze mirrors. *Cult Relics*. 1992;12:79–90 (In Chinese).
35. Coccato A, Costa M, Rousaki A, Clist BO, Karklins K, Bostoen K, et al. Micro-Raman spectroscopy and complementary techniques (hXRF, VP-SEM-EDS, μ -FTIR and Py-GC/MS) applied to the study of beads from the Kongo Kingdom (Democratic Republic of the Congo). *J Raman Spectrosc*. 2017;48(11):1468–78. <https://doi.org/10.1002/jrs.5106>.
36. Zmuda-Trzebiatowska I, Schaefer K, Sokolowska A, Rodzik I, Sobczyk AT, Karczewski J, Sliwinski G. Raman investigation of the patina layers on Hungarian copper ingots from a fifteenth century shipwreck. *J Raman Spectrosc*. 2016;47(12):1528–33. <https://doi.org/10.1002/jrs.5059>.
37. Echavarria A, Echeverria F, Arroyave C, Gil H. Study of the copper corrosion mechanism in the presence of propionic acid vapors. *J Braz Chem Soc*. 2009;20:1841–8. <https://doi.org/10.1590/S0103-50532009001000011>.
38. Luo W. Analysis of bronzes excavated in ancient Jun. Taiwan: University of Science and Technology of China; 2008. (In Chinese).
39. Yu B, Fang J, Huang E. Characteristics of the Raman spectra of archaeological Malachites. *J Raman Spectrosc*. 2013;44(4):630–6. <https://doi.org/10.1002/jrs.4230>.
40. Privitera A, Corbascio A, Calcani G, Ventura GD, Ricci MA, Sodo A. Raman approach to the forensic study of bronze patinas. *J Archaeol Sci Rep*. 2021;39: 103115. <https://doi.org/10.1016/j.jasrep.2021.103115>.
41. Ingo GM, Riccucci C, Giuliani C, Faustoferri A, Pierigel FG, Pascucci M, Albini M, Carlo GD. Surface studies of patinas and metallurgical features of uncommon high-tin bronze artefacts from the Italic necropolises of ancient Abruzzo (Central Italy). *Appl Surf Sci*. 2019;470:74–83. <https://doi.org/10.1016/j.apsusc.2018.11.115>.
42. Makreški P, Jovanovski G, Dimitrovska S. Minerals from Macedonia: XIV. Identification of some sulfate minerals by vibrational (infrared and Raman) spectroscopy. *Vib Spectrosc*. 2006;39(2):229–39. <https://doi.org/10.1016/j.vibspec.2005.04.008>.
43. Hayez V, Guillaume J, Hubin A, Terryn H. Micro-Raman spectroscopy for the study of corrosion products on copper alloys: setting up of a reference database and studying works of art. *J Raman Spectrosc*. 2005;35(8–9):732–8. <https://doi.org/10.1002/jrs.1194>.
44. McNeil MB, Mohr DW. Sulfate formation during corrosion of copper alloy objects. *MRS Online Proc Libr*. 1992;267:1047–53. <https://doi.org/10.1557/PROC-267-1047>.
45. Frost RL, Williams PA, Martens W, Leverett P, Klopogrog JT. Raman spectroscopy of basic copper(II) and some complex copper(II) sulfate minerals: Implications for hydrogen bonding. *Am Miner*. 2004;89(7):1130–7. <https://doi.org/10.2138/am-2004-0726>.

46. Ferreira LFV, Gomesb MV, Pereirac MFC, Santosd LF, Machadoae IF. A multi-technique study for the spectroscopic characterization of the ceramics from Santa Maria do Castelo church (Torres Novas, Portugal). *J Archaeol Sci Rep*. 2016;6:182–9. <https://doi.org/10.1016/j.jasrep.2016.02.013>.
47. McCann LL, Trentelman K, Possley T, Golding B. Corrosion of ancient Chinese bronze money trees studied by Raman microscopy. *J Raman Spectrosc*. 1999;30(2):121–32.
48. Luo W, Qin Y, Huang F, Hu Y, Wang C. Study of corrosion products on bronzes excavated from Hubei. *Corros Sci Prot Technol*. 2007;3:157–61 (**In Chinese**).
49. Mu Y, Luo W, Li L, Huang F, Wang C. Analysis on layered structure of corrosion products on west Zhou bronzes excavated from Yejiashan, Suizhou, Hubei. London: Hindawi Publishing Corporation; 2020. p. 8–16 (**In Chinese**).

Publisher's Note

Springer Nature remains neutral with regard to jurisdictional claims in published maps and institutional affiliations.

Submit your manuscript to a SpringerOpen[®] journal and benefit from:

- ▶ Convenient online submission
- ▶ Rigorous peer review
- ▶ Open access: articles freely available online
- ▶ High visibility within the field
- ▶ Retaining the copyright to your article

Submit your next manuscript at ▶ [springeropen.com](https://www.springeropen.com)
